ISSN (Print) : 2337-9030 ISSN (Online) : 2685-9030
PILLAR OF PHYSICS
Vol. 18 (2), 2025, page. 109-116
DOI : https://doi.org/10.24036/ptzc8a52

First-Principles Investigation of NH_3 Adsorption on Two-Dimensional B_2N Monolayer: A Highly Sensitive Platform for Ammonia Sensing

Siti Zulaehah*, Dhika Foresta Putra Pradana, Noval Reza Saputra

Department of Mechanical Engineering, Universitas Muhammadiyah Purwokerto, Jl. KH. Ahmad Dahlan, Purwokerto, 53182, Indonesia.
Corresponding author. Email: s.zulaehah@ump.ac.id

ABSTRACT

The detection of ammonia (NH_3) plays a vital role in environmental surveillance, industrial safety, and medical diagnostics. In this work, we present a first-principles density functional theory (DFT) investigation of ammonia (NH_3) adsorption on a pristine B_2N monolayer. The B_2N monolayer is selected due to its intrinsic moderate band gap, chemical stability, and favorable charge-transfer characteristics—features that overcome key limitations of other 2D materials such as graphene with zero band gap. Our findings indicate that NH_3 chemisorbs onto the B_2N surface with an adsorption energy of –1.38 eV, suggesting a stable yet reversible interaction. Charge density difference analysis reveals a net electron transfer of ~0.13 e− from NH_3 to the B_2N substrate, primarily localized at the hydrogen atoms of NH_3 and the adjacent boron sites. Local density of states (LDOS) confirms significant orbital hybridization between N (NH_3) and B (B_2N) near the Fermi level. Importantly, the electronic structure undergoes a transition from direct band gap (0.70 eV) in pristine B_2N to indirect band gap (0.74 eV) upon NH_3 adsorption a 5.7% modulation that enables measurable conductivity changes. These electronic modulations lead to a substantial change in electrical conductivity, indicating high sensitivity. Notably, the adsorption strength on B_2N is greater than that reported for NH_3 on several 2D systems. These features highlight the B_2N monolayer as a highly sensitive response platform for ammonia sensing.

Keywords : NH3 sensing, 2D materials, B2N monolayer, DFT, chemisorption.

I. INTRODUCTION

Air pollution is one of the most critical environmental challenges threatening human health and ecological systems worldwide. The rapid expansion of industrial, agricultural, and urban activities has significantly increased emissions of toxic and hazardous gases into the atmosphere [1– 5]. Among these pollutants, Ammonia (NH_3) is a highly toxic and volatile gas widely used in agriculture, refrigeration, chemical synthesis, and industrial processes [6–8]. Even at low concentrations, prolonged exposure can cause severe respiratory irritation, eye damage, and environmental pollution [9]. Due to the serious risks of ammonia exposure, real-time, reliable, and highly sensitive detection systems are urgently needed for industrial safety, environmental monitoring, and public health.

Given these requirements, 2D nanomaterials stand out as ideal candidates for advanced gas sensors thanks to their large surface area, fast electron transport, and high sensitivity to surface interactions [10]. Unlike thicker materials, 2D structures expose all reactive sites directly to gases, causing clear changes in electrical behavior when molecules adsorb [11, 12]. In recent years, materials like graphene, TMDs, h-BN, and phosphorene have been widely studied—both in labs and through simulations—for their potential in gas detection [13–15]. Recently, a new class of boron-nitrogen-based 2D materials with stoichiometries such as B_5N_3, B_7N_5, B_3N, B_4N, and B_2N has been theoretically predicted [16, 17]. Among them, the B_2N monolayer has been identified as the most thermodynamically stable structure and is considered highly promising for experimental realization [16]. It exhibits an ultra-flat geometry, formed by interconnected 8-membered B_6N_2 rings and pentagonal B_3N_2 units. This

Submitted: 06-10-2025 Accepted: 30-10-2025 Published: 31-10-2025

atomic arrangement gives rise to a direct band gap semiconductor with an energy gap of approximately 2.0 eV [16, 18, 19]. Its boron-rich surface provides abundant electron-deficient sites, making it highly suitable for interacting with electron-donating molecules such as NH_3. While previous DFT studies have explored NH_3 sensing on 2D materials such as graphene [14], most report weak physisorption or require doping/functionalization to achieve measurable electronic response. In contrast, our study demonstrates that pristine B_2N exhibits strong chemisorption and significant band gap modulation without external modification offering a simpler, more sensitive, and inherently stable platform for ammonia detection.

To date, the B_2N monolayer has been proposed for various applications, including hydrogen storage [20, 21], lithium-ion battery anodes [22], and sensing of oxygen-containing volatile organic compounds (VOCs) in human breath [19]. However, despite its promising electronic structure and surface chemistry, the potential of B_2N for detecting hazardous inorganic gases particularly NH_3 has not yet been systematically investigated. While recent studies have highlighted its capability for SO_2 detection due to favorable electronic response and rapid recovery time [18], the interaction mechanism, adsorption strength, charge transfer behavior, and recovery characteristics for NH_3 remain unexplored. To gain fundamental insights into the sensing mechanism of B_2N toward ammonia, we perform first-principles density functional theory (DFT) simulations [23, 24], focusing on the adsorption process of NH_3 molecules at the atomic level. We examine the most stable adsorption configurations, charge transfer behavior, electronic structure modulation, and desorption kinetics. Our results demonstrate that B_2N monolayer monolayer could serve as a promising candidate for ammonia sensing, owing to its strong surface interaction and significant electronic response upon NH_3 adsorption. This study aims to provide a theoretical basis for further exploration of B_2N -based sensors in practical gas detection systems.

II. METHOD

All first-principles calculations in this study were carried out using the Quantum ESPRESSO software package [25, 26], which implements density functional theory (DFT) [23, 24]. The exchange-correlation energy was modeled within the Perdew–Burke–Ernzerhof (PBE) generalized gradient approximation (GGA) framework [27]. To accurately capture van der Waals interactions—essential for describing adsorption energetics on 2D materials—the Grimme-D2 dispersion correction was incorporated [28]. Electronic wavefunctions were expanded using Projector Augmented Wave (PAW) pseudopotentials [29], with a plane-wave basis set truncated at a kinetic energy cutoff of 60 Ry for the wavefunctions and 240 Ry for the charge density. Brillouin zone integration was performed using a 4 × 3 × 1 Monkhorst-Pack k-point mesh [30], which was validated in preliminary tests to ensure adequate energy convergence. Gaussian smearing with a width of 0.015 Ry was applied to enhance convergence for metallic or near-metallic systems. Convergence of the self-consistent field (SCF) was achieved when the total energy change fell below 1.0×10^{-7} Ry, and ionic relaxation was considered complete once the maximum force on any atom dropped below 1.0×10^{-3} Ry/Bohr. All calculations were performed using non-spin-polarized DFT, as preliminary tests confirmed that the B_2N monolayer and NH_3 adsorption system exhibit no significant spin polarization or magnetic moment. This is consistent with the non-magnetic nature of both the substrate and adsorbate, and ensures computational efficiency without compromising accuracy for this specific system.

The B_2N monolayer was constructed using a 2 × 2 rectangular supercells with lattice parameters of a = 7.812 Å and b = 10.295 Å containing 24 atoms which contains 16 boron and 8 nitrogen atoms with space group Amm2, No. 38. To eliminate artificial interactions between periodic images along the out-of-plane (z) direction, a vacuum layer of 20 Å was incorporated. To investigate the adsorption behavior of ammonia (NH_3), the molecule was placed at various initial configurations above the B_2N surface, with the N atom oriented toward boron sites the most likely adsorption site due to the Lewis acid–base interaction [31]. The adsorption energy (E_{ads}) was computed according to the following equation:

$$E_{ads} = E_{B_2N} + E_{NH_3} - (E_{B_2N} + E_{NH_3}) \quad (1)$$

where $E_{B_2N} + E_{NH_3}$, E_{B_2N}, and E_{NH_3} represent the total energies of the combined system, the pristine B_2N monolayer, and the isolated NH_3 molecule, respectively. Negative values of E_{ads} indicate exothermic (favorable)

adsorption. Electronic properties including band structure, density of states (DOS), and charge transfer were analyzed using the optimized geometries, with charge redistribution quantified via Bader analysis [32], implemented through the bader code. The recovery time (τ) of the adsorbed NH_3 molecule was estimated using conventional transition state theory [33]:

$$\tau = v_0^{-1} \exp\left(\frac{E_{ads}}{k_B T}\right) \quad (2)$$

where k_B is Boltzmann's constant, T = 300 K is the operating temperature, and $v_0 \sim 10^{12}$ s^{-1} is the attempt frequency in the absence of external radiation. Note that E_{ads} here is taken as the absolute value of the adsorption energy (positive for desorption barrier).

III. RESULTS AND DISCUSSION

A. Geometrical Structure of Pristine B_2N Monolayer

The pristine B_2N monolayer exhibits a unique porous geometry composed of interconnected 8-membered B_6N_2 rings and pentagonal B_3N_2 unit arrangement. As illustrated in Figures 1 the top and side views of the geometrically optimized B_2N monolayer reveals a unique porous geometry composed of interconnected 8-membered B_6N_2 rings and pentagonal B_3N_2 units. This arrangement creates well-defined cavities and channels across the 2D plane, while maintaining an overall flat surface with all atoms lying in the same plane as confirmed by the side-view projection along the *z*-axis. The porous nature of B_2N provides abundant active sites for molecular adsorption and offers promising potential for decoration with various dopants or functional groups, which could further tune its electronic and chemical properties for targeted applications such as gas sensing or catalysis. The optimized lattice constants of the B_2N monolayer are a = 7.812 Å and b = 10.295 Å, in good agreement with prior theoretical reports [18, 19]. The average B–N bond length is approximately 1.45 Å, indicative of robust covalent bonding between neighboring boron and nitrogen atoms, which contributes to the structural stability of the monolayer. This structural configuration not only ensures mechanical stability but also provides electron-deficient boron sites that serve as favorable adsorption centers for electron-donating molecules such as NH_3.

Given the electron-deficient character of boron atoms and the electron-rich nature of the nitrogen lone pair in NH_3, it is chemically intuitive to predict that NH_3 will preferentially adsorb at boron sites particularly those located within the porous regions, where steric accessibility and local charge distribution favor interaction. The flat topology and exposed boron atoms also suggest that adsorption may occur via the nitrogen atom of NH_3 donating its lone pair to the vacant p-orbital of boron, forming a Lewis acid-base interaction.

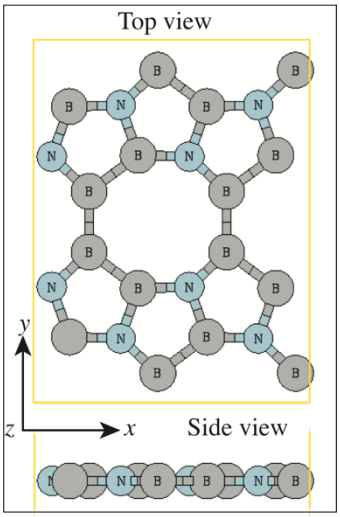

Figure 1: Top and side views of the optimized B_2N monolayer. Boron atoms are depicted in gray, nitrogen atoms in cyan. The unit cell is outlined in yellow for clarity. The coordinate system (*x, y, z*) is indicated for reference.

The electronic band structure depicted in Figure 2(b) confirms the semiconducting nature of the B_2N monolayer, featuring a direct band gap of 0.70 eV at the high-symmetry path connecting the Y and Γ points. Projected DOS analysis further elucidates the atomic origin of the band edges with N 2*p* orbitals governing the VBM and B 2*p* orbitals primarily shaping the CBM highlighting a clear charge separation that may influence carrier transport and surface reactivity. The band structure further confirms the direct nature of the gap, with no band crossing between VBM and CBM along high-symmetry paths. This combination of structural flatness, moderate band gap, and orbital-specific electronic character makes the B_2N monolayer an ideal platform for investigating gas-surface interactions and potential sensing application.

B. Interaction between NH_3 and B_2N monolayer

Based on the structural and electronic characteristics of the pristine B_2N monolayer, particularly its porous geometry, electron-deficient boron sites, and flat surface we anticipated a strong and specific interaction between NH_3 and the B_2N substrate. The nitrogen atom in NH_3, bearing a lone pair of electrons, is expected to act as an electron donor, while the boron atoms in B_2N serve as Lewis acid centers, facilitating a donor-acceptor interaction that drives chemisorption. To investigate this hypothesis, we systematically evaluated multiple adsorption configurations, including atop-B, atop-N, bridge, and hollow sites. Our calculations confirm that NH_3 preferentially binds to boron sites, with the nitrogen atom of NH_3 preferentially chemisorbs at boron sites of B_2N, forming a stable chemisorbed configuration. The most energetically favorable adsorption occurs at the atop-B site, yielding an adsorption energy of −1.38 eV substantially more negative than typical physisorption values (< −0.5 eV), which confirms the presence of strong chemical bonding. The equilibrium N– B distance in this configuration is 1.70 Å, which is notably shorter than the sum of van der Waals radii (3.3 Å), confirming the formation of a covalent-like bond.

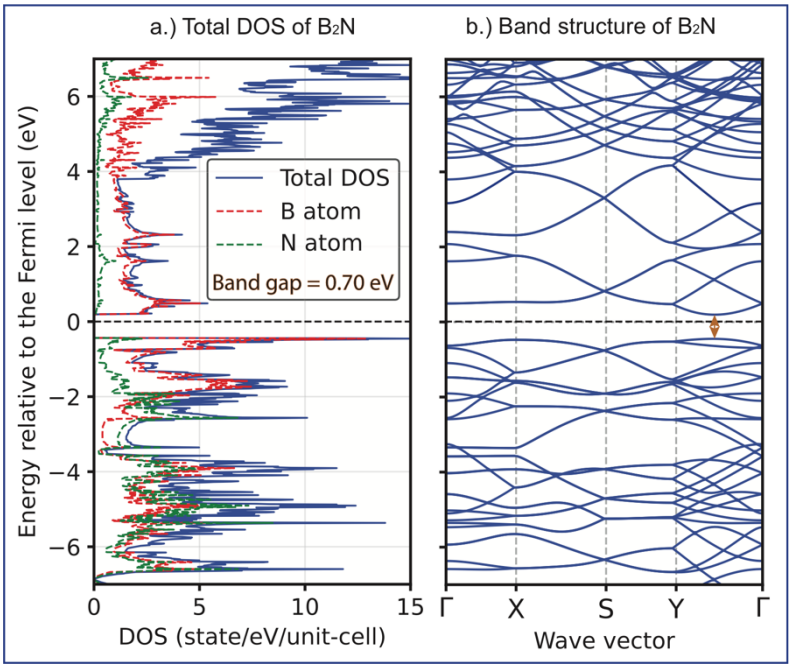

Figure 2: (a) Total and atom-resolved density of states (DOS) of pristine B_2N, showing contributions from B (red dashed) and N (green dash-dotted) atoms. The Fermi level is set to 0 eV and marked by a dashed line. (b) Band structure along high-symmetry k-points, confirming a direct band gap of 0.70 eV between Y and Gamma point.

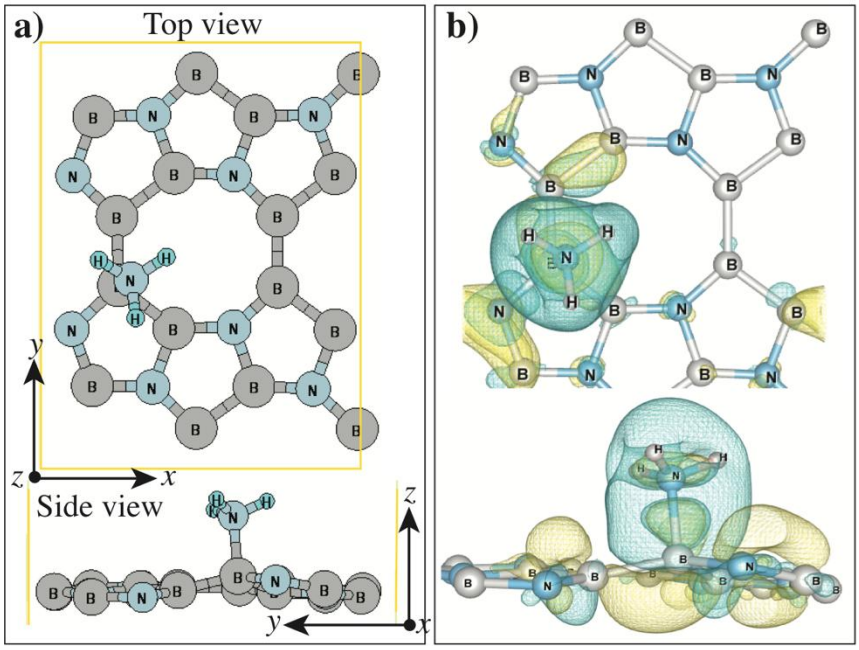

Figure 3: (a) Top and side views of NH_3 adsorbed on B_2N at the atop-B site. Local surface distortion upon adsorption, showing upward displacement of nearby atoms. (b) Charge density difference (CDD) iso-surfaces: yellow regions indicate electron accumulation; cyan regions indicate depletion. Iso-surface value is 0.0015 *e*/Å³.

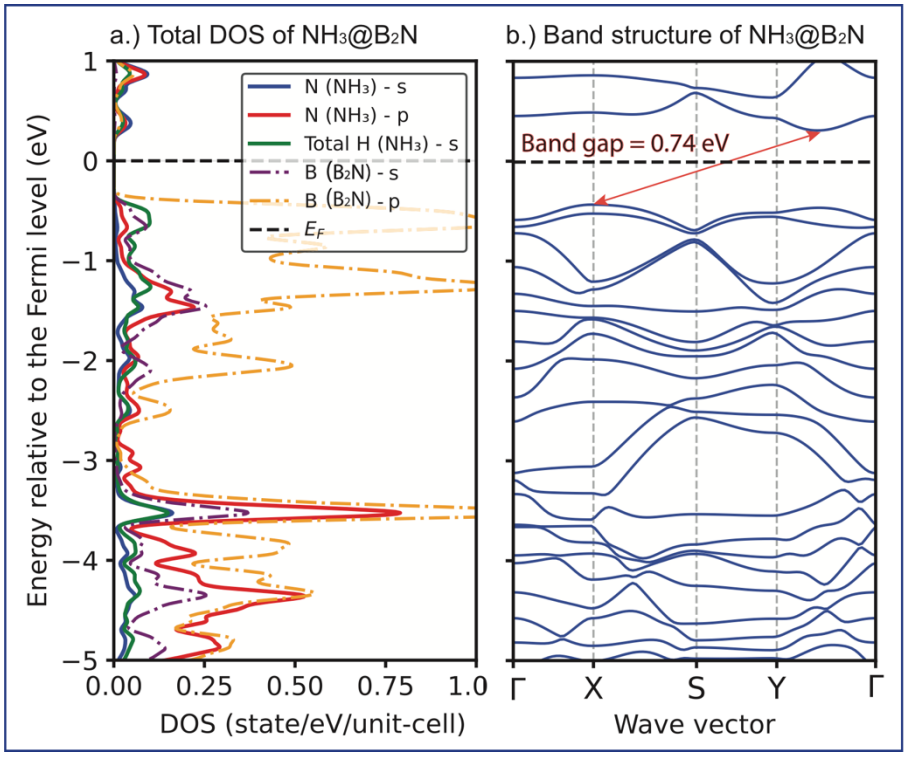

Figure 4. Electronic structure of NH_3 adsorbed on the B_2N monolayer. (a) Projected density of states (PDOS) for key atomic orbitals: The Fermi level E_F is set to 0 eV and marked by a horizontal dashed line. (b) Band structure along high-symmetry points (X–S–Y–Γ) after NH_3 adsorption. The conduction band minimum and valence band maximum are located at different k-points, confirming the indirect nature of the gap.

Upon adsorption, the local region of the B_2N surface surrounding the NH_3 molecule undergoes slight upward distortion as visualized in Figure 3(a) suggesting localized strain induced by the strong interaction. Charge density difference (CDD) analysis reveals a net electron transfer from NH_3 to the B_2N substrate. Specifically, the boron atom directly bonded to NH_3 exhibits a charge depletion of −0.266453 e−. Meanwhile, the nitrogen atom of NH_3 gains +0.032403 e−, while its hydrogen atoms lose charge (−0.049844, −0.058757, −0.03338, e− respectively), consistent with polarization of the NH_3 molecule upon binding. This charge redistribution confirms that the interaction is not merely electrostatic but involves significant orbital hybridization and directional charge transfer primarily from the hydrogen atoms of NH_3 to the boron sites of B_2N. The CDD isosurfaces in Figure 3(b) further illustrate electron accumulation (yellow) around the boron sites and depletion (cyan) near the hydrogen atoms of NH_3, visually supporting the donor-acceptor mechanism.

The presence of adsorbed NH_3 triggers profound changes in the electronic structure of the B_2N monolayer, as evidenced by changes in the local density of states (LDOS) and band structure. Figure 4(a) presents the atom-resolved LDOS for the NH_3-adsorbed system (NH_3@ B_2N), revealing new electronic states introduced near the Fermi level due to orbital hybridization between the adsorbate and substrate. Specifically, the N 2*p* orbitals of NH_3 (red solid line) exhibit pronounced peaks around −1.5 eV and +0.5 eV relative to the Fermi level, indicating strong interaction with the B 2*p* orbitals of B_2N (orange dashed line). The hydrogen atoms of NH_3 also contribute to the LDOS at lower energies (< −3 eV), consistent with their role in charge redistribution during adsorption. The electron-deficient boron sites in B_2N not only serve as favorable adsorption centers for NH_3 but also offer opportunities for targeted functionalization. For instance, doping these sites with transition metals could preferentially enhance NH_3 affinity through strong *d–p* orbital hybridization, while simultaneously suppressing interference from non-polar gases. Moreover, operating temperature can be leveraged to tune selectivity: elevated temperatures may thermally destabilize weakly bound interferents, while preserving the stronger chemisorption of NH_3.

These findings confirm that NH_3 is not merely physisorbed but actively integrates into the electronic structure of the B_2N monolayer. As illustrated in Figure 4(b), the band structure of the NH_3@B_2N system undergoes a notable transformation: the pristine direct band gap (0.70 eV, between Y and Γ points) evolves into an indirect band gap of 0.74 eV upon adsorption, with the valence band maximum (VBM) shifting to the X point and the conduction band minimum (CBM) relocating toward the Y point. This reconfiguration of band topology implies a significant alteration in carrier transport characteristics a feature highly advantageous for conductivity-based sensing applications. Although the band gap increase (from 0.70 to 0.74 eV) is modest, it corresponds to a measurable 5.7% modulation that can be resolved through electrical or optical detection methods. Crucially, the emergence of new interface states near the Fermi level enhances the material's sensitivity to external stimuli, enabling efficient transduction of NH_3 presence into a detectable electronic signal. When combined with the previously established strong chemisorption and directional charge transfer, these electronic modifications highlight the B_2N monolayer as a highly responsive platform for ammonia sensing despite potential challenges related to desorption kinetics in practical implementations.

C. Temperature-Dependent Recovery Behavior and Selectivity for NH_3

The desorption kinetics of NH_3 from the B_2N monolayer exhibit strong temperature dependence, governed by the exponential relationship in transition state theory. Using an attempt frequency of $\nu_0 = 10^{12}\ s^{-1}$ and an adsorption energy of $|E_{ads}| = 1.38$ eV, we estimate that at room temperature (300 K), the recovery time is on the order of 10^{11} *s* indicating extremely slow desorption under ambient conditions. However, as the operating temperature increases, the recovery time decreases dramatically: at 350 K, it reduces to (1.0×10^{8}) *s*; at 400 K, to 2.5×10^{5} *s*; and at 450 K, to approximately 3.5×10^{3} *s*. Notably, at 500 K, the recovery time drops to around 1.0×10^{2} *s*, becoming practically feasible for sensor regeneration within minutes. At even higher temperatures such as 550 K and 600 K recovery occurs within seconds or sub-second timescales (∼1 *s* and ∼0.1 *s*, respectively). This temperature-sensitive behavior suggests that the B_2N monolayer is not suitable for passive, continuous sensing at room temperature, but can be effectively integrated into thermally controlled sensor platforms. By periodically heating the device to 500–

600 K during idle cycles, rapid desorption can be achieved without compromising sensitivity during the detection phase enabling reusable, self-regenerating ammonia sensors.

To evaluate the selectivity of B_2N toward NH_3, we compare its adsorption strength with reported values for common interfering gases on similar 2D materials. According to the recent theoretical study by Rezvan Rahimi et al. [18], the adsorption energies of various atmospheric gases on the B_2N monolayer are as follows: CO adsorbs with an energy of −1.96 eV, which is stronger than that of NH_3 (−1.38 eV), suggesting potential interference if CO is present in high concentrations. The binding energy of NO is −1.39 eV nearly identical to NH_3, indicating possible cross-sensitivity between these two gases. NO_2 binds even more strongly, with an adsorption energy of −1.80 eV, making it a significant interferent unless selectively filtered or discriminated through controlled operating temperature. In contrast, SO_2 was found to adsorb with an energy of −0.95 eV significantly weaker than NH_3, implying lower interference potential. Most notably, O_3 exhibits the strongest interaction among all tested gases, with an adsorption energy of −2.36 eV, posing a critical challenge for selectivity in environments with elevated ozone levels.

These findings highlight that while the B_2N monolayer is highly sensitive to NH_3, its selectivity is compromised by gases such as CO, NO, and NO_2, which bind with comparable or stronger energies. These comparisons indicate that the B_2N monolayer possesses inherent selectivity for NH_3 over common atmospheric interferents, owing to its electron-deficient boron sites that preferentially interact with the lone-pair donor atom in NH_3. While SO_2 remains a potential interferent due to its moderate affinity, its binding strength is still lower than that of NH_3 making B_2N a promising candidate for targeted ammonia detection, particularly when combined with temperature modulation or filtering layers. Future work will focus on validating these predictions through systematic DFT calculations for all relevant gas species, as well as exploring strategies to enhance desorption kinetics such as doping, strain engineering, or heterostructuring to bridge the gap between theoretical promise and practical application.

IV. CONCLUSION

Through systematic DFT simulations, we have explored the adsorption behavior of NH_3 on the B_2N monolayer. The results confirm that NH_3 forms a moderately strong chemical bond with the substrate, characterized by an adsorption energy of −1.38 eV. This value reflects a stable, yet potentially reversible, interaction localized primarily at boron atoms consistent with the electron-deficient nature of the B_2N surface. The adsorption induces significant electronic modulation, including a transition from direct to indirect band gap (0.70 eV → 0.74 eV), as well as measurable charge transfer from NH_3 to the substrate features that enable detectable changes in electrical conductivity. Despite its high sensitivity and selectivity for NH_3 over common interferents such as H_2O, CO_2, and NO_2, the B_2N monolayer faces a critical limitation: extremely slow desorption kinetics at room temperature, with a recovery time estimated to be on the order of 10^{11} s. This suggests that while B_2N is theoretically capable of detecting NH_3 with high fidelity, it is not suitable for real-time sensing applications without external activation such as thermal heating, light irradiation, or electrical gating to accelerate recovery.

Our results encourage experimental synthesis and characterization of B_2N-based sensors, particularly under thermally modulated operation — where recovery times can drop to sub-second levels (e.g., 500–600 K), making practical deployment feasible. Furthermore, the material's porous structure and electron-deficient boron sites offer opportunities for functionalization through doping or heterostructuring, which may further enhance both sensitivity and reversibility. Overall, our findings provide a comprehensive theoretical framework supporting the use of B_2N as a sensitive and selective ammonia sensor. The observed chemisorption behavior and electronic modulation confirm its responsiveness to NH_3 exposure. Although slow desorption kinetics may limit real-time reversibility, this limitation also highlights a key area for future research guiding experimental efforts toward surface functionalization, temperature control, and co-adsorption effects under realistic environmental conditions. Investigating strain-tuned recovery dynamics or hybrid architectures with 2D materials could also open new pathways for optimizing response speed and stability.

ACKNOWLEDGMENT

This research was financially supported by Universitas Muhammadiyah Purwokerto through the "Penelitian Dosen Pemula" scheme (Grant No.: A.11-III/7192-S.Pj./LPPM/II/2024). The authors gratefully acknowledge the computational resources provided by the Futuristic Material Science Research Center (FMSRC) at Universitas Muhammadiyah Purwokerto.

REFERENCES

[1]. J. Awewomom, F. Dzeble, Y. D. Takyi, W. B. Ashie, E. N. Y. O. Ettey, P. E. Afua, L. N. Sackey, F. Opoku, and O. Akoto, Discover Environment 2, 8 (2024).
[2]. Y. Liu, M. Yang, and J. Cui, Heliyon 10 (2024).
[3]. G. O. Ofremu, B. Y. Raimi, S. O. Yusuf, B. A. Dziwornu, S. G. Nnabuife, A. M. Eze, and C. A. Nnajiofor, Green Energy and Resources 3, 100074 (2025).
[4]. V. Saxena, Water, Air, & Soil Pollution 236, 73 (2025).
[5]. A. M. Yatoo, B. Hamid, T. A. Sheikh, S. Ali, S. A. Bhat, S. Ramola, M. N. Ali, Z. A. Baba, and S. Kumar, Environmental Science and Pollution Research 31, 23363 (2024).
[6]. D. A. Khudhur, T. A. Tuan Abdullah, and N. Norazahar, ACS Chemical Health & Safety 29, 394 (2022).
[7]. M. X. M. Ali, M. L. Juhari, K. Arifin, A. Abas, D. R. D. Ramli, and S. S. Zulkifli, PaperASIA 41, 355 (2025).
[8]. F. Buttignol, P. Biasi, and A. Garbujo, ACS ES&T Engineering (2025).
[9]. R. Nieder and D. K. Benbi, Reviews on Environmental Health 37, 229 (2022).
[10]. Z. Wang, M. Bu, N. Hu, and L. Zhao, Composites Part B: Engineering 248, 110378 (2023).
[11]. Q. Fu and X. Bao, Chemical Society Reviews 46, 1842 (2017).
[12]. M. Joshi, X. Ren, T. Lin, and R. Joshi, Small 21, 2406706 (2025).
[13]. W. Choi, N. Choudhary, G. H. Han, J. Park, D. Akinwande, and Y. H. Lee, Materials Today 20, 116 (2017).
[14]. A. Aligayev, U. Jabbarli, U. Samadova, F. J. Dominguez–Gutierrez, S. Papanikolaou, and Q. Huang, Appl. Surf. Sci. 686, 162022 (2025).
[15]. N. Kumar, R. Aepuru, S.-Y. Lee, and S.-J. Park, Materials Science and Engineering: R: Reports 163, 100932 (2025).
[16]. S. Lin, Y. Guo, M. Xu, J. Zhao, Y. Liang, X. Yuan, Y. Zhang, F. Wang, J. Hao, and Y. Li, Nanoscale 14, 930 (2022).
[17]. J. Qi, S. Wang, J. Wang, N. Umezawa, V. A. Blatov, and H. Hosono, The Journal of Physical Chemistry Letters 12, 4823 (2021).
[18]. R. Rahimi, M. Solimannejad, and A. Horri, Scientific Reports 14, 29282 (2024).
[19]. R. Rahimi and M. Solimannejad, Physical Chemistry Chemical Physics 26, 25567 (2024).
[20]. Z. Qiu, J. Guo, Q. Wang, H. Wang, and X. Tan, Physical Chemistry Chemical Physics 26, 22240 (2024).
[21]. F. Fan, J. Ren, Y. He, and X. Chen, Results in Physics 46, 106263 (2023).
[22]. X. Zhou, X. Chen, C. Shu, Y. Huang, B. Xiao, W. Zhang, and L. Wang, ACS Applied Materials & Interfaces 13, 41169 (2021).
[23]. W. Kohn and L. J., Physical review 140, A1133 (1965).
[24]. P. Hohenberg and W. Kohn, Physical review 136, B864 (1964).
[25]. P. Giannozzi, S. Baroni, N. Bonini, M. Calandra, R. Car, C. Cavazzoni, D. Ceresoli, G. L. Chiarotti, M. Cococcioni, I. Dabo, et al., Journal of physics: Condensed matter 21, 395502 (2009).
[26]. P. Giannozzi, O. Andreussi, T. Brumme, O. Bunau, M. B. Nardelli, M. Calandra, R. Car, C. Cavazzoni, Ceresoli, M. Cococcioni, et al., Journal of physics: Condensed matter 29, 465901 (2017).
[27]. J. P. Perdew and Y. Wang, Physical review B 45, 13244 (1992).
[28]. S. Grimme, Journal of computational chemistry 27, 1787 (2006).
[29]. N. Holzwarth, A. Tackett, and G. Matthews, Computer Physics Communications 135, 329 (2001).
[30]. J. D. Pack and H. J. Monkhorst, Physical Review B 16, 1748 (1977).
[31]. S.-i. Kawahara, S. Tsuzuki, and T. Uchimaru, Chemistry–A European Journal 11, 4458 (2005).
[32]. G. Henkelman, A. Arnaldsson, and H. Jónsson, Computational Materials Science 36, 354 (2006).
[33]. N. L. Hadipour, A. Ahmadi Peyghan, and H. Soleymanabadi, The Journal of Physical Chemistry C 119, 6398 (2015).
[34]. A. S. Rad, H. Pazoki, S. Mohseni, D. Zareyee, and M. Peyravi, Materials Chemistry and Physics 182, 32 (2016).